FFEMS Fatigue & Fracture of Engineering Materials & Structures

doi: 10.1111/ffe.12052

Probabilistic sensitivity analysis of dwell-fatigue crack initiation life for a two-grain microstructural model

D. M. SPARKMAN[1], H. R. MILLWATER[1] and S. GHOSH[2]

[1]*The University of Texas at San Antonio, San Antonio, TX, 78249, USA,* [2]*The Johns Hopkins University, Baltimore, MD, 21218, USA*

Received in final form 13 June 2012

ABSTRACT Crack initiation in Ti-6242 has been observed to occur in a grain with a hard orientation for basal slip neighbouring a grain with a soft orientation. Because there is significant variability in microstructural features and crack initiation life, it is useful to explore the effects of the variability of the microstructural components through a probabilistic sensitivity analysis. In this paper, a probabilistic crystal plasticity finite element model of a hard–soft grain combination (2 grains) was exercised considering the Schmid factor of the soft grain, the misorientation angle between the two grains, and the soft grain size as random variables. A probabilistic sensitivity analysis of the time-to-crack initiation was then employed in order to ascertain the relative importance of the random variables. The results indicate that the variance in the Schmid factor accounts for the majority of the variance in the time-to-crack initiation. A local sensitivity analysis found that larger Schmid factors result in smaller mean life and larger variance. The neighbouring soft grain size was found to be less important than the Schmid factor and misorientation angle.

Keywords dwell fatigue; crack formation; probabilistic sensitivity analysis; titanium alloy.

NOMENCLATURE

B, c, γ_s = crack opening displacement, micro-crack length, surface energy
$\mathbf{C}$ = anisotropic elasticity tensor
d = number of dimensions of the input space (i.e. the number of random variablesof the training data)
D = Soft grain size
E^e = Green-Lagrange strain tensor
$E[\,]$, $V[\,]$ = expected value operator, variance operator
F_j = linearised cumulative density function of variable X_j
F, F^e, F^p = deformation gradient, elastic component, plastic component
G, b, g_0^α = elastic shear modulus, Burgers vector, initial deformation resistance
b^β, $q^{\alpha\beta}$ = self hardening rate, latent hardening matrix
h_0^β, g_s^β = initial hardening rate, saturation slip deformation resistance
K_{mix}, K_n, K_t, K_c = mixed mode, normal, shear, and critical stress intensity factors
L^p = plastic velocity gradient
n = number of samples in the training data
P = Applied stress
PDF, CDF = probability density function, cumulative distribution function
$r, \widetilde{g}, n$ = slip system hardening parameters
R, R_c = crack initiation parameter, critical crack initiation parameter
s = a sample from the training data represented as a location in the input space,with coordinates given in values of the input variables
s_0^α, m_0^α, n_0^α = Schmid tensor, slip direction, and slip plane normal of the α th slip system
SF = Schmid Factor
S_i, S_{Ti} = first order sensitivity index, total effects sensitivity index
t_f = time-to-crack-initiation

Correspondence: Harry R. Millwater, Jr. Email: Harry.Millwater@utsa.edu

u = interpolation point, a sample location in the input space in which the value ofthe response is to be predicted
$Z(s)$ = value of the response evaluated at a sample of the training data
β, T_n, T_t = shear stress factor, normal stress, shear stress
$\dot{\gamma}^\alpha \tilde{\dot{\gamma}}^\alpha$ = plastic shearing rate, reference plastic shearing rate
θ_{mis} = Misorientation angle
$\kappa_{Fj}(x)$ = local kernel function
λ = kriging weights
λ^β ,Λ = slip plane lattice incompatibility measure, Nye's dislocation density tensor
$\mu(s)$ = mean function
τ^α, g^α = αth slip system resolved shear stress, slip system deformation resistance
σ, S = Cauchy, second Piola-Kirchoff stresses
χ^α, m = back-stress, material rate sensitivity parameter

INTRODUCTION

The life of some titanium alloys is known to be significantly reduced under dwell fatigue as compared with normal fatigue.[1,4] Titanium alloys are generally classified into three categories, α, $\alpha+\beta$ and β, depending on the relative presence of the α phase, which has a hexagonal close-packed crystal structure, and the β phase, which is body-centred cubic.[2] Examples of the $\alpha+\beta$ alloys include Ti-6Al-4V and Ti-6242 and are often used in aircraft engines. Both alloys are processed such that the predominant phase is primary alpha (α_P).

The low symmetry of the hexagonal close-packed crystal structure and the elastic and plastic anisotropy of the α phase have important consequences for the yield strength, creep and fatigue life of titanium alloys. The deformation of titanium alloys is known to be sensitive to crystallographic texture[3] and microtexture.[4] The local crystallographic orientations of the alpha grains effect the distribution of micro-stresses within the microstructure.[5] Localised plastic slip near a grain boundary causes plastic incompatibility and stress concentration.[6] Grain faceting studies have shown that crack initiation sites in the alpha phase of titanium alloys occur most often in grains that are 'hard' oriented for basal slip (c-axis near-parallel to the loading direction). When a hard grain is neighboured by 'soft' grains that are oriented for easier slip (c-axis at ~45° to the loading direction), this is termed a rogue grain combination.[7,8] This orientation mismatch has been suggested to lead to load-shedding in the soft grain and corresponding redistribution of the load onto the hard grain. A crack initiation criterion[9] based on the load-shedding phenomenon and the micro-crack-like behaviour of edge dislocation pile-up at grain boundaries has recently been proposed. This crack initiation mechanism has been called load-shedding,[9] quasi-cleavage[8] or pseudo-cleavage.[23]

Some studies have observed facet planes with normal vectors near 45° from the loading direction.[22,23] The slip systems with slip planes coplanar with the facet surface have a high corresponding Schmid factor. In these cases, the faceted grains were oriented for easy slip suggesting that facet formation was induced by plastic slip within the faceted grain. This slip-induced crack formation mechanism is fundamentally different than the quasi-cleavage mechanism and is not addressed by the criterion in Ref. [9].

The crack initiation criterion in Ref. [9] is currently being applied with the two-grain crystal plasticity finite element model seen in Fig. 1 to study the crack initiation life of Ti-6242. Following a traditional sensitivity analysis, the *values* of the Schmid factor (for basal slip) of the soft grain (SF), the misorientation angle between the two grains (θ_{mis}), and the soft grain size (D) were studied for their effect on the *value* of the crack initiation life (time-to-failure (t_f)) of the hard grain. In a specimen of Ti-6242 with no texture, each of the hard grains will be neighboured by softer grains with random values of the Schmid factor, misorientation angle and grain size. The uncertainty in these variables was quantified with probability distributions. The distributions for these parameters are described in the section titled Input Random Variables.

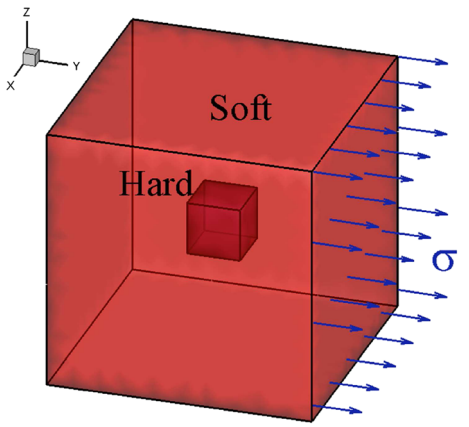

Fig. 1 Statistical volume element of a two grain system used for crack nucleation studies.

The focus of this paper is on the application of probabilistic sensitivity methods to determine how the *joint distribution* of these input variables affects the *distribution* of the crack initiation life for dwell fatigue and creep conditions. In this work, the bicrystal model of the hard–soft grain combination is studied, and its crack initiation probabilistic sensitivity results will be compared with crack initiation observations in the literature.

The distributions from the bulk material were used to approximate the distributions of these variables for a random grain neighbouring a hard grain. This approximation is assumed appropriate because of the absence of texture. This study is for the crack initiation life of hard-oriented alpha grains in titanium alloys. Specifically, only the faceting of alpha grains that are hard-oriented for basal slip by quasi-cleavage is considered using the criterion in Ref. [9].

The slip-induced mode of crack initiation is not investigated in this study. Also, the effect of the lamellar $\alpha+\beta$ grains is not considered. Crack nucleation in the alpha grains in a titanium alloy has been found to be affected by micro-texture.[10] The consequences of texture and micro-texture on crack initiation life are not addressed in this work.

A probabilistic sensitivity analysis offers a more comprehensive analysis of the sensitivity than traditional deterministic methods because all random variables are allowed to vary simultaneously rather than a local derivative approach based on an expansion point. There are multiple probabilistic sensitivity methods that can be employed such as visual (scatter plots, parallel coordinate plots), score function,[11] global sensitivity analysis[12] and others. In this work, scatter plots, global sensitivity analysis methods and a local probabilistic analysis method[13] were employed within a Monte Carlo probabilistic analysis. These methods offer a robust assessment of the importance of the random variables towards the variability of the crack initiation life.

The computational expense of the two-grain crystal plasticity finite element model and crack initiation criterion described in the section on the Two-grain Microstructural Model prohibits the use of direct Monte Carlo simulation-based sensitivity methods. Therefore, a kriging metamodel surrogate was developed to circumvent this obstacle by providing an efficient mathematical function relating numerical values of the random variables (Schmid factor, misorientation, soft grain size) to an approximate time-to-crack initiation. This surrogate was then used for Monte Carlo sampling. The development of the kriging model is described in the section on Kriging. With the kriging metamodel, the time-to-crack initiation is efficiently predicted given values for *SF*, θ_{mis} and *D*, allowing for a large number of samples to be obtained for a global sensitivity analysis. The sensitivity methods are described in the section on Probabilistic Sensitivity Analysis and the probabilistic sensitivity results are presented in the section titled Results and Discussion.

TWO-GRAIN MICROSTRUCTURAL MODEL

Crystal plasticity finite element model

An isothermal, size-dependent and rate-dependent crystal plasticity finite-element computational model described and developed in Refs. [3,14,15] was used in conjunction with an in-house parallelized code to simulate the response of microstructures of the α Ti-6242. The α phase consisted of equiaxed grains with an *hcp* structure. Detailed description of these computational models is presented in Refs. [3,14,15] and only summarised in this section. In this model, crystal deformation results from a combination of the elastic stretching and rotation of the crystal lattice and plastic slip on the different slip systems. The model incorporates the basal, prismatic, pyramidal <a>, and pyramidal <c + a> slip systems. The stress–strain relation in this model is written in terms of the second Piola–Kirchoff stress ($S = \det F^e F^{e-1} \sigma F^{e-T}$) and the work conjugate Green–Lagrange strain tensor ($E^e \equiv (1/2)\{F^{eT}F^e - I\}$) as follows:

$$S = C : E^e \tag{1}$$

where $\boldsymbol{C}$ is the fourth order anisotropic elasticity tensor, σ is the Cauchy stress tensor and F^e is the elastic deformation gradient defined by the relation

$$F^e = FF^{p-1},\ \det F^e > 0 \tag{2}$$

F and F^p are the deformation gradient and its plastic component, respectively with the incompressibility constraint $\det F^p = 1$. The flow rule governing evolution of plastic deformation is expressed in terms of the plastic velocity gradient as follows:

$$L^p = \dot{F}^p F^{p-1} = \sum_{\alpha} \dot{\gamma}^{\alpha} s_0^{\alpha} \tag{3}$$

where the Schmid tensor is expressed as $s_0^{\alpha} \equiv m_0^{\alpha} \otimes n_0^{\alpha}$ in terms of the slip direction (m_0^{α}) and slip plane normal (n_0^{α}) in the reference configuration, associated with αth slip system. The plastic shearing rate $\dot{\gamma}^{\alpha}$ on the αth slip system is given by the power law relation as

$$\dot{\gamma}^{\alpha} = \dot{\bar{\gamma}} \left| \frac{\tau^{\alpha} - \chi^{\alpha}}{g^{\alpha}} \right|^{1/m} \operatorname{sign}(\tau^{\alpha} - \chi^{\alpha}),\quad \tau^{\alpha} \equiv (C^e : E) \cdot s_0^{\alpha} \tag{4}$$

Here, $\dot{\bar{\gamma}}$ is the reference plastic shearing rate, τ^{α} and g^{α} are the αth slip system resolved shear stress and the slip system

deformation resistance respectively, χ^α is the back-stress that accounts for kinematic hardening in cyclic deformation, m is the material rate sensitivity parameter and C^e is the elastic stretch. The evolution of the slip system deformation resistance is assumed to be controlled by both statistically stored dislocations corresponding to homogenous plastic deformation and geometrically necessary dislocations (GNDs) that accommodate the incompatibility of the plastic strain field. This is expressed as

$$\dot{g}^\alpha = \sum_\beta q^{\alpha\beta} h^\beta \left|\dot{\gamma}^\beta\right| + \frac{k_0 \alpha^2 G^2 b}{2\left(g^\alpha - g_0^\alpha\right)} \sum_\beta \lambda^\beta \left|\dot{\gamma}^\beta\right| \qquad (5)$$

where h^β in the first term of Eq. (5) is self-hardening rate and $q^{\alpha\beta}$ is a matrix describing the latent hardening. The evolution of the self-hardening rate is assumed to be governed by the relation

$$h^\beta = h_0^\beta \left|1 - \frac{g^\beta}{g_s^\beta}\right|^r \operatorname{sign}\left(1 - \frac{g^\beta}{g_s^\beta}\right), \quad g_s^\beta = \tilde{g}\left(\frac{\dot{\gamma}^\beta}{\tilde{\dot{\gamma}}}\right)^n \qquad (6)$$

where h_0^β is the initial hardening rate, g_s^β is the saturation slip deformation resistance, and r, $\tilde{g}$ and n are the slip system hardening parameters. The second term of Eq. (5) accounts for the effect of GNDs on the work hardening, in which k_0 is a dimensionless material constant, G is the elastic shear modulus, b is the Burgers vector, g_0^α is the initial deformation resistance and α is a non-dimensional constant taken to be 1/3 in this work. λ^β is a slip plane lattice incompatibility measure, which can be expressed for each slip system as a function of slip plane normal (n^β) and another incompatibility tensor (Λ) as

$$\lambda^\beta = \left(\Lambda n^\beta \bullet \Lambda n^\beta\right)^{1/2} \qquad (7)$$

The Nye's dislocation density tensor Λ is a direct measure of GND density. Nye's tensor can be expressed using the curl of the plastic part of the deformation gradient tensor F^P. This crystal plasticity formulation calculates the dislocation density tensor as $\Lambda = -\frac{1}{b}\left(\nabla \times F^{pT}\right)^T$.

The dependence of initial slip system deformation resistances on grain size for individual slip systems have been expressed using Hall–Petch type relations in Ref. [15]. Different slips are grouped as soft and hard slip modes, depending on the nature of slip transmission, and the characteristic length for each slip system is defined accordingly. The slip system deformation resistance of individual slip systems is obtained from the values calibrated from corresponding single crystal experiments in Refs. [3,14]. The accuracy of the size-dependent model is established by comparing the simulation results for constant strain rate and creep tests in tension and compression with experiments in Ref. [15].

For the bicrystal model in Fig. 1 plasticity was allowed in both the hard-oriented and soft-oriented grains. The hard-oriented grain (inner cube) was discretized into a mesh of 1296 linear tetrahedron elements. The soft-oriented (outer cube) has a mesh of 15 168 elements. A mesh convergence study was performed to optimise the macroscopic and microscopic responses. For boundary conditions, a stress condition was applied on one face and otherwise minimum constraints were applied to suppress rigid body modes.

Dwell fatigue crack nucleation model

Morphological and crystallographic characteristics of the microstructure, e.g. crystal orientations, misorientations and grain size distribution, play significant roles in the mechanical behaviour and fatigue failure response. A material microstructure-based detailed mechanistic model for fatigue crack nucleation has been developed in Refs. [9,16,21]. This model is at the length scale of individual grains and is set for each hard grain−soft grain combination in the polycrystalline aggregate. It is non-local in the sense that while the crack nucleates in the hard grain due to load shedding, it is affected by plasticity in the neighbouring soft grains due to dislocation pile-ups at grain boundary barriers. The transgranular crack nucleation model is built on the premise that a wedge crack nucleates in the neighbouring grain as a dislocation approaches the grain boundary. An edge dislocation, which is an extra half plane of atoms wedged between two complete planes, is equivalent to a micro-crack with opening displacement of one atomic spacing b. As more dislocations are piled up, the opening displacement increases in size as shown in Fig. 2a. The crack opening displacement corresponds to the closure failure along a circuit, surrounding the piled-up dislocations. If n edge dislocations of Burger's vector b, contribute to the formation of a micro-crack, a wedge with opening displacement $B = nb$ is produced. It should be noted that while the dislocations are piled up at the grain boundary of a soft grain, the wedge crack initiates in the adjacent hard grain as shown in Fig. 2b.

As demonstrated in Fig. 2a, the micro-crack length c can be considered as the length after which the disturbance in the lattice structure of the hard grain subsides. This disturbance is caused by extra half planes of atoms in the soft grain. The equilibrium length of a wedge crack with an opening displacement B is related to the elastic properties and surface energy γ_s as follows:

$$c = \frac{G}{8\pi(1-\upsilon)\gamma_s} B^2 \qquad (8)$$

where υ is the Poisson's ratio and G is the shear modulus. The wedge crack is initially stable. As more dislocations

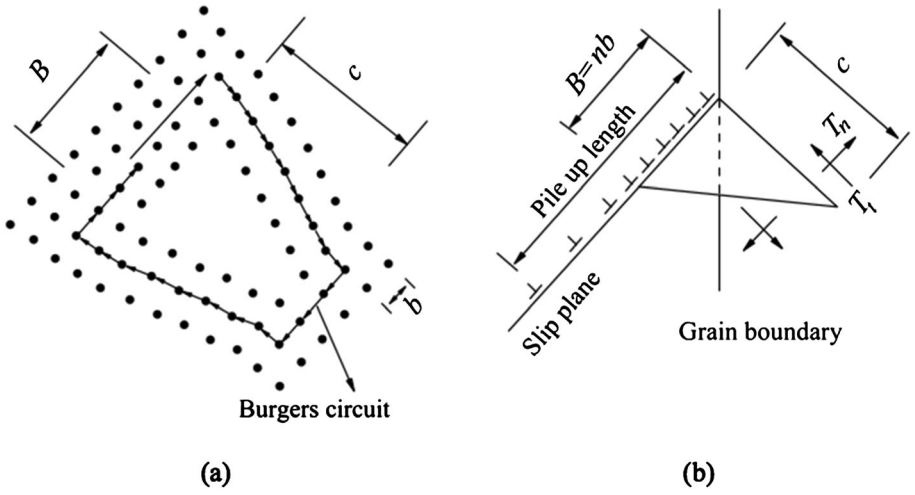

Fig. 2 (a) A wedge crack with opening displacement of $4b$, produced by coalescence of four dislocations, (b) nucleation of a wedge crack in the hard grain resulting from a dislocation pile up in the soft grain.

enter the crack, the crack opening size increases and, therefore, the crack length also increases. However, the applied stress across the micro-crack, which is associated with the hard grain, will also help open up the crack. The acting stress on the micro-crack surface is a combination of normal and shear stresses as shown in Fig. 2b. The micro-crack becomes unstable when the mixed mode stress intensity factor K_{mix} exceeds a critical value K_c. K_{mix} is expressed in terms of normal stress intensity factor K_n and shear stress intensity factor K_t as

$$K_{mix} = \sqrt{K_n^2 + \beta K_t^2} \tag{9}$$

β is a shear stress factor, which is used to assign different weights to the normal and shear traction components for mixed mode. It is defined as the ratio of the shear to normal fracture toughness of the material, i.e. $\beta \approx K_{nc}/K_{tc}$. Using the definitions for stress intensity factors $K_n = \langle T_n \rangle \sqrt{\pi c}$ and $K_t = T_t \sqrt{\pi c}$ and noting that the micro-crack grows when $K_{mix} \geq K_c$, the hard grain crack nucleation criterion, ahead of dislocation pile-ups in adjacent soft grain is stated as $T_{eff} = \sqrt{\langle T_n \rangle^2 + \beta T_t^2} \geq \frac{K_c}{\sqrt{\pi c}}$, or equivalently

$$R = T_{eff}\sqrt{c} \geq R_c, \text{ where } R_c = \frac{K_c}{\sqrt{\pi}} \tag{10}$$

T_{eff} is an effective stress for mixed mode crack nucleation. The stress component normal to the crack surface is given as $T_n = n_i^b \left(\sigma_{ij} n_j^b\right)$, in terms of the Cauchy stress tensor σ_{ij}, and the components of unit outward normal to the slip plane n_i^b. Only the tensile normal stress $\langle T_n \rangle$, represented by the McCauley bracket $\langle\rangle$, contributes to the effective stress because compressive stresses do not contribute to crack opening. The shear stress component T_t is obtained by the vector subtraction of T_n from the stress vector on the plane, i.e. $T_t\, t^b = T - T_n n^b$ where t^b is the unit vector tangent to the plane. The typical values of c that give rise to an unstable cracking are of the order of nanometers whereas the typical grain size is of the order of microns. Thus, it is reasonable to consider the maximum stress at the grain boundary of the hard grain as the remote stress. R_c is a parameter that depends on the material elastic properties, as well as on the critical strain energy release rate G_c. It has the units of stress intensity factor (MPa$\sqrt{\mu m}$). A value of $\beta = 0.7071$ for Ti-alloys is used in this study. Sensitivity analysis with different values of β indicate that T_{eff} is not very sensitive to β for $<c+a>$ oriented hard grains, because $T_n >> T_t$. As more dislocations are added to the pile-up with time, the wedge crack opening displacement and length increase. This implies that a smaller T_{eff} is needed to initiate a crack with increasing plastic deformation and pile-up. This contributes to the non-locality aspect of the crack nucleation criterion.

The time-to-crack initiation is determined by advancing the crystal plasticity finite element analysis incrementally in time until the value of R exceeds the value of R_c for the hard–soft grain pair combination.

INPUT RANDOM VARIABLES

Each of the grains oriented for hard basal slip in a specimen of Ti-6242 is neighboured by a collection of grains with different crystallographic orientations and sizes. This results in uncertain values of the soft grain basal Schmid factor (SF), misorientation angle between the two grains (θ_{mis}), and the soft grain size (D). Given a hard

grain, the fraction of its contact area with a neighbouring soft grain serves as an estimate of the probability of having a neighbour with the soft grain's characteristics. Histograms were developed for the largest basal SF, θ_{mis} and D from orientation data of a 600-grain microstructure of Ti-6242. The $\alpha+\beta$ phase colony regions were homogenised in the manner of of Deka *et al.* in Ref. [14]. From these histograms, cumulative distribution functions (CDFs) were developed for use with the sensitivity methods described in the section on Probabilistic Sensitivity Analysis. The histograms and corresponding CDFs are given in Figs 3–5. These CDFs were sampled during the Monte Carlo sampling described in the section on Results and Discussion.

The Schmid factor distribution in Fig. 3 is bounded on both sides and exhibits negative skewness; larger values of Schmid factor in the neighbouring soft grain are more likely to occur. The misorientation angle distribution in Fig. 4 shows that a neighbouring soft grain is more likely to have a medium to large misorientation with the hard grain than a small misorientation. The grain size (described by equivalent sphere diameter) distribution in Fig. 5 shows that a neighbouring soft grain has a distribution centred about 14 μm, bounded on both sides. These distributions were sampled as non-parametric, i.e. standard probability distributions (e.g. normal, lognormal, beta, etc.) were not fit to these distributions. Table 1 gives the first and second moments and coefficient of variation of each random variable.

The cube-shaped hard-oriented grain in the model in Fig. 1 is an idealisation of the shape of an actual grain in a microstructure. Grain shape and spatial orientation are variables not considered in this study.

KRIGING

A kriging metamodel was developed that relates the largest Schmid factor of the basal slip systems, misorientation angle and soft grain size (the input variables) to the time-to-crack initiation (the response). This mathematical model then served as a surrogate during the Monte Carlo sampling. Kriging is an interpolation method from geostatistics based on work by D. Krige and subsequently further developed by G. Matheron and others[17] and has in recent years been extensively applied to surrogate modelling of computer experiments.[18,19]

Development of a kriging metamodel follows the following steps:

1 Select samples for the training data set, s (design of experiments);
2 Evaluate the 'true' response for each sample of s (observe);
3 Estimate the hyper-parameters of the mean and covariance functions (inference); and
4 Evaluate the kriging metamodel at the prediction locations u for $Z(u)$ (predict).

Kriging metamodel

Given a set of training data that is assumed to be a realization of a random field, the best estimate of the response at a prediction location is the expected value of the random field at that location. This results in a kriging metamodel of the form

$$Z(u) \approx \mu(u) + \lambda^T [Z(s) - \mu(s)] \tag{11}$$

The response $Z(u)$ is predicted by a trend function $\mu(\bullet)$, the kriging weights λ and the residuals between the 'true' values and the trend predictions $[Z(s) - \mu(s)]$. The training data s is the $n \times d$ matrix of samples with observed 'true' response value $Z(s)$, where n is the number of samples and d is the number of dimensions of the input space. The first term in Eq. (11) contains $\mu(u)$, which is a scalar value. The second term contains

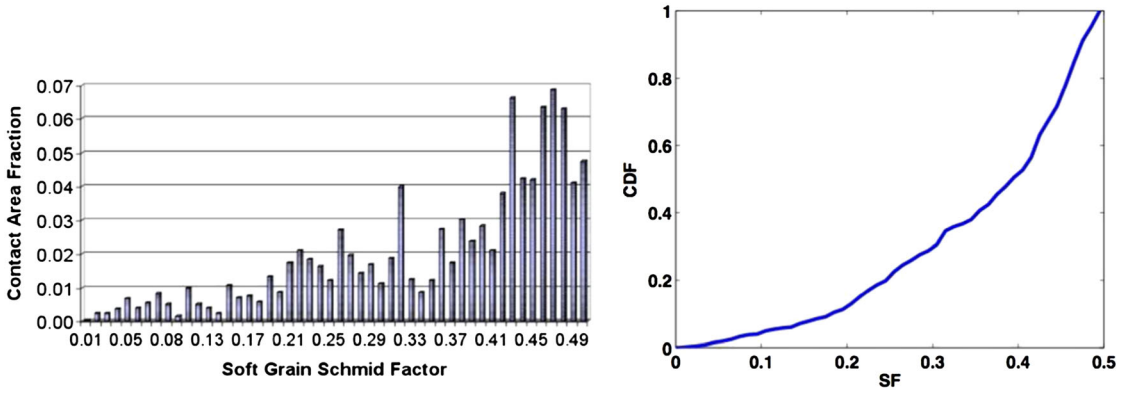

Fig. 3 Schmid factor distribution.

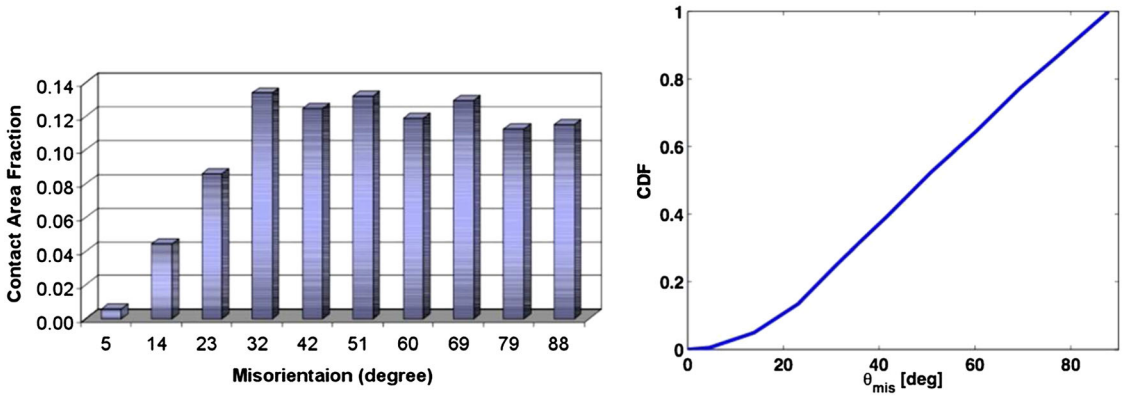

Fig. 4 Misorientation angle distribution.

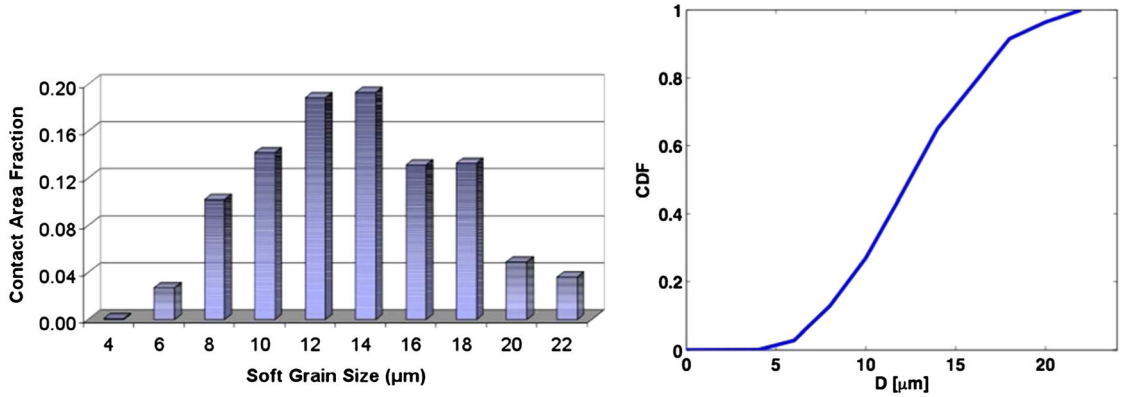

Fig. 5 Grain size distribution.

Table 1 Moment estimates of input variables

Variable	Schmid factor	Misorientation angle	Grain size
	SF	θ_{mis}	*D*
μ	0.38	53.7	13.6
σ	0.118	21.9	3.96
c.o.v.	0.33	0.41	0.29

c.o.v., coefficient of variation.

λ, $Z(s)$ and $\mu(s)$, which are all n x 1 column vectors. It is important to point out that s (and u) are vectors of the input variables for the metamodel. The input variables (and response) are not required to have Gaussian distributions even though with kriging, the response is assumed to be a Gaussian random field.

With the calibrated kriging metamodel, it is possible to efficiently obtain an approximate value for the response given a set of realisations of the input variables. This allows estimation of the distribution of the response with Monte Carlo sampling. Scatter plots and probabilistic sensitivities were also developed to investigate the sources of uncertainty in the response distribution.

PROBABILISTIC SENSITIVITY ANALYSIS

Sensitivity analysis is defined as 'the study of how uncertainty in the output of a model can be apportioned to different sources of uncertainty in the model input'.[12] The results of a sensitivity analysis can be used to rank the importance of input variables, identify critical regions in the space of the input variables, and aid in verification, and validation of models.[12]

The probabilistic sensitivity methods used in this paper are scatter plots, global sensitivity analysis with variance-based sensitivity indices, and a localised sensitivity analysis.

Scatter plots

Scatter plots are two-dimensional Cartesian point plots of realisations of a random variable versus the model output. The purpose of a scatter plot is to determine visually

if there is a relationship between the particular input and output variables in the plot. If the variable is not important, the cloud of points will largely reflect the randomness of the input random variable. Conversely, if the random variable is important, the cloud of points will indicate some relationship between input and output.

Global sensitivity analysis – first order and total effects indices

Objectives of a global sensitivity analysis (GSA) are to identify the important input variables of a model and to quantify their relative importance. The basis behind GSA is to apportion the variance of the output among the input random variables. The basic element of GSA is to determine the reduction in the output variance if a random variable is fixed at a specific value, i.e. its variability is eliminated. If an input random variable has a large influence on the variance of the output, then the variance of the output will reduce considerably when the variable is fixed. Conversely, for an unimportant random variable, the variance of the output will change little when the variable is fixed. As a result, the conditioned variance, normalised by the unconditioned variance, provides a qualitative indicator as to variable importance. In order to provide a quantitative estimate, an expected value is taken over all conditioned values. This variance-based method is 'model free' and thus is applicable to models of any form and any level of linearity and any distribution type. Also they are global as they incorporate the influence of the full distribution of the input variables.

Consider a model with output Y that is a function of a vector on input random variables X. In this case, $Y = Y(X)$. Variance describes the amount of uncertainty in the value of a variable and is given by

$$V[Y] = E\left[(Y - E[Y])^2\right] \tag{12}$$

The law of total variance decomposes the variance into an expected conditional variance and the variance of a conditional expectation.

$$V[Y] = E_{X_i}\left[V_{X_{\sim i}}\left(Y\middle|X_i = x_i^*\right)\right] + V_{X_i}\left[E_{X_{\sim i}}\left(Y\middle|X_i = x_i^*\right)\right] \tag{13}$$

where X_i is the ith input random variable.

The first term in the right hand side of Eq. (13) is the variance of the output conditioned on the input variable X_i being fixed at a value of x_i^*, then averaged over all of X_i, which is indicated by the E_{X_i}. The second term in Eq. (13) is the variance over all of X_i of the average output conditioned on the input variable X_i being fixed. The subscripts $_{X_i}$ and $_{X_{\sim i}}$ indicate that the operations E or V are carried out with respect to variable X_i and all variables except X_i, respectively.

If the expected conditional variance of Y for X_i is small relative to $V[Y]$, then X_i is an important variable because, on average, the variance of Y is decreased significantly when the variance of X_i is removed. Conversely, the variance of the average, $V_{X_i}\left[E_{X_{\sim i}}(Y|X_i)\right]$, will then be larger, closer in value to $V[Y]$. Normalising by $V[Y]$ gives what is called the first order effects sensitivity index, which gives the main effect contribution of each input variable to the variance of the output.[12]

$$S_i = \frac{V_{X_i}\left[E_{X_{\sim i}}(Y|X_i)\right]}{V[Y]} \tag{14}$$

The total effect index for variable X_i is a measure of the total contribution of the variation of the input X_i to the variation of the output. It includes the first order effects and all higher order effects from interactions with other variables and is determined by subtracting all the variance due to the other variables with[12]

$$S_{T_i} = 1 - \frac{V\left[E\left(Y\middle|X_{\sim i}\right)\right]}{V[Y]} \tag{15}$$

If the total effect index for a variable is large relative to the first order index, then interactions with the other variables significantly affect the variance of the response. Conversely, if the total effect index for a variable is zero, then the variance of that variable is of no importance in the problem.

Global sensitivity analysis has an attractive mathematical property that for independent random variables, the sum of all the first order and higher indices will be equal to 1. The sum of all first-order effects, S_i, will be approximately equal to 1 if there are negligible interactions of the variables in the model.

After both the first-order indices and total effect indices are calculated for each of the input variables, they can be compared to identify the relative importance of each variable. Larger values of S_i and S_{Ti} denote greater relative importance.

Localised sensitivity analysis

Global sensitivity analysis gives a measure of the relative importance of each variable based on the contribution of its variance to the output variance. However, it does not address which 'region' of the random variable is more important, e.g. the left tail, central region or right tail.

The relative importance of 'regions' within each of the random variables may be determined with a method recently proposed by Millwater, *et al.*[13] for independent random variables. This method gives the sensitivity of the response mean, μ_Y or standard deviation, σ_Y, to a local change in the linearised CDF, F_j, of variable X_j. The concept is shown schematically in Fig. 6. The sensitivity of the response mean to a local change in the CDF is

$$\frac{\partial \mu_Y}{\partial F_j} = \int_{-\infty}^{\infty} Y(x)\kappa_{F_j}(x) f_x(x) dx = E\left[Y(x)\kappa_{F_j}(x)\right] \quad (16)$$

where $\kappa_{F_j}(x)$ is a local kernel function. The sensitivity of the standard deviation of the response to a local change in the linearised CDF of a variable is

$$\frac{\partial \sigma_Y}{\partial F_j} = \frac{E\left[Y(x)^2\kappa_{F_j}(x)\right] - 2\mu_Y E\left[Y(x)\kappa_{F_j}(x)\right]}{2\sigma_Y} \quad (17)$$

The local change in the distribution amounts to a small shift of the local density from higher values to lower values (shift *left*) of the variable of interest (Fig. 7). A first-order approximation of the change in the moment of the response due to a local shift to the *right* of the density of the input variable is found with the negative of the sensitivity.

$$\text{Shift Probability Density Left} : \frac{\partial \mu_Y}{\partial F_j}, \frac{\partial \sigma_Y}{\partial F_j} \quad (18)$$

$$\text{Shift Probability Density Right} : -\frac{\partial \mu_Y}{\partial F_j}, -\frac{\partial \sigma_Y}{\partial F_j} \quad (19)$$

An interesting aspect is that this method allows direct comparison of regions of *different* variables, because the

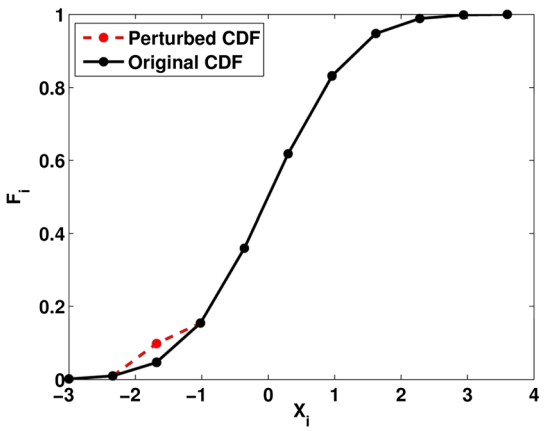

Fig. 6 Localised sensitivity method – CDF.

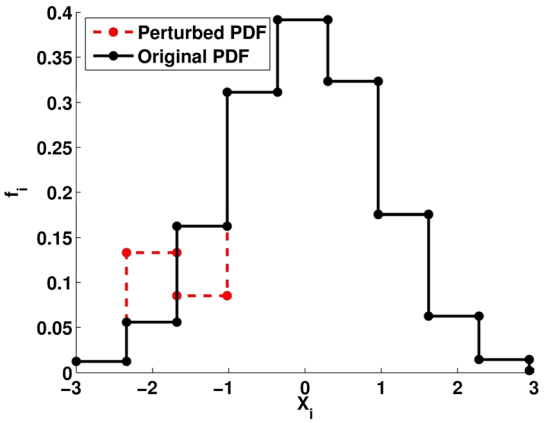

Fig. 7 Localised sensitivity method – PDF.

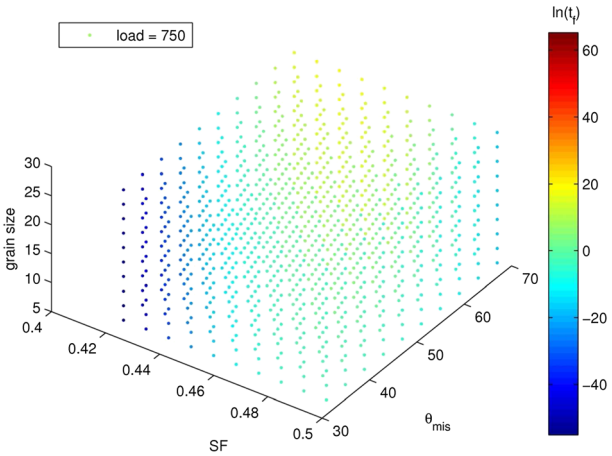

Fig. 8 Predicted values of $\ln(t_f)$ for $P = 750$ MPa.

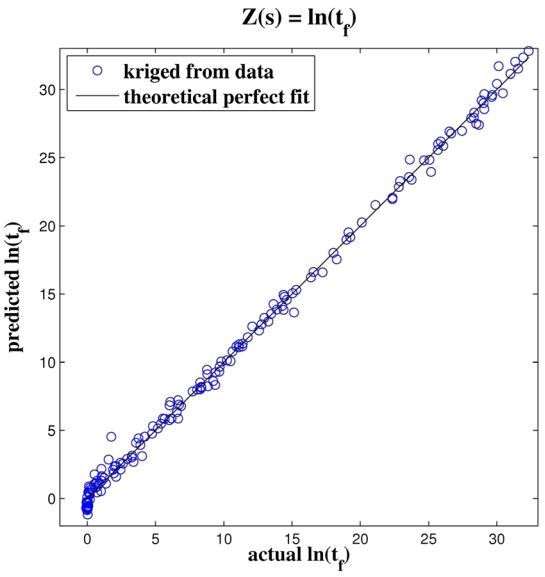

Fig. 9 Predicted values of $\ln(t_f)$ with respect to actual values – cross validation.

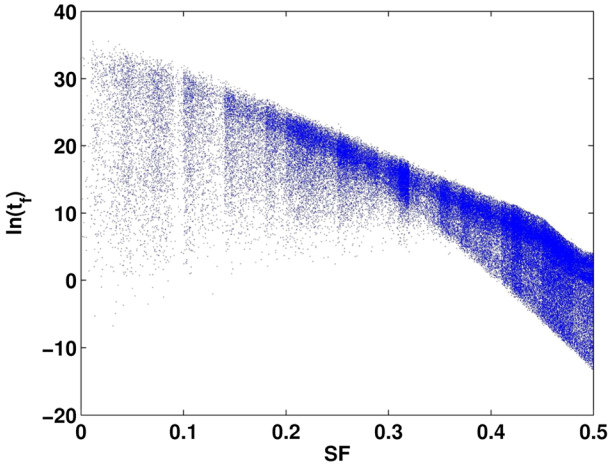

Fig. 10 Scatter plot of $\ln(t_f)$ with respect to Schmid factor for 750 MPa.

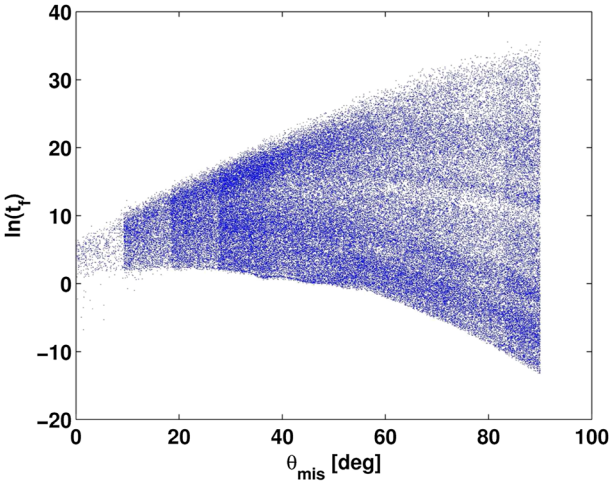

Fig. 11 Scatter plot of $\ln(t_f)$ with respect to misorientation angle for 750 MPa.

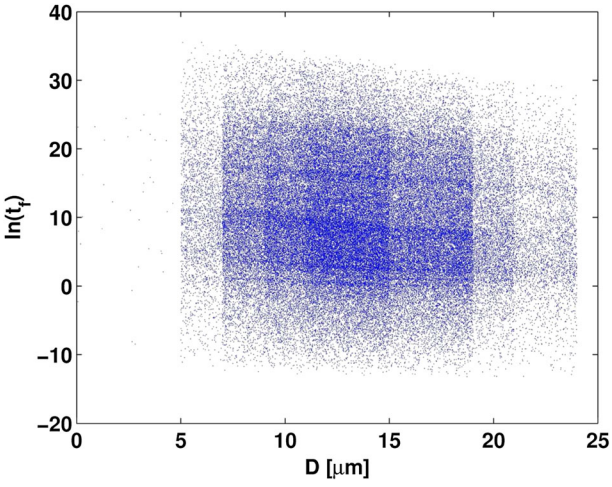

Fig. 12 Scatter plot of $\ln(t_f)$ with respect to grain size for 750 MPa.

sensitivities are of the response with respect to the CDF of the input variable.

RESULTS AND DISCUSSION

Kriging model

One hundred eighty-three evaluations of the two-grain crystal plasticity finite element model were executed considering various values of the input random variables (Schmid factor *SF*, misorientation angle θ_{mis} and soft grain size *D*) and the applied load, *P*, to obtain times-to-crack initiation. A kriging model was developed using these results to predict crack initiation life for other values of the input variables. Because of the large changes in the order of magnitude of t_f (15 orders of magnitude) over the samples tested, the response t_f was transformed for kriging such that $Z(s) = \ln(t_f)$. A Matern I correlation function was selected on the basis of the best overall fit as measured by R^2 in cross validation tests. Maximum likelihood estimation was used to fit the trend function

Table 2 Moment estimates of transformed time-to-crack-initiation for various loads

Variable	Transformed time-to-crack-initiation		
	$\ln(t_f)$		
	$P = 450$ MPa	$P = 750$ MPa	$P = 900$ MPa
μ	41.9	9.6	1.9
σ	12.7	8.6	6.7
c.o.v.	0.3	0.9	3.5

c.o.v., coefficient of variation.

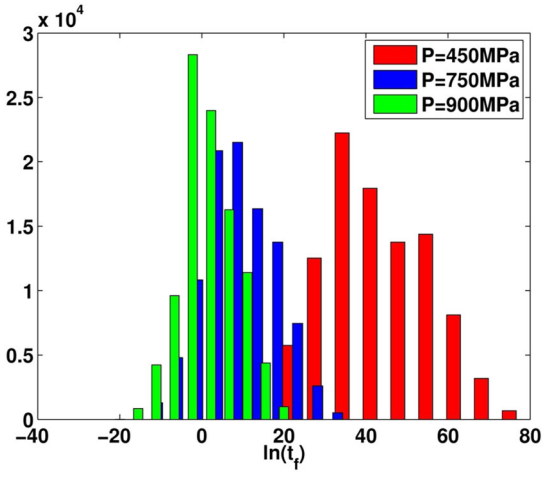

Fig. 13 Histograms of $\ln(t_f)$ for various loads.

Table 3 Sensitivity indices for $\ln(t_f)$ for various loads

Sensitivity index	S_i			S_{T_i}		
Variable	Schmid factor	Misorientation angle	Grain size	Schmid factor	Misorientation angle	Grain size
Load [MPa]	SF	θ_{mis}	D	SF	θ_{mis}	D
450	0.8658	0.0585	0.0130	0.9367	0.1006	−0.0024
500	0.8648	0.0418	0.0030	0.9399	0.1589	0.0386
550	0.8550	0.0487	0.0142	0.9330	0.1257	−0.0013
600	0.8367	0.0277	−0.0113	0.9558	0.1938	0.0549
650	0.8195	0.0680	0.00228	0.9219	0.1411	−0.0105
700	0.8131	0.0419	0.0144	0.9381	0.1660	0.0021
750	0.8036	0.0470	0.0146	0.9395	0.1854	0.0011
800	0.7712	0.0500	0.0075	0.9444	0.2193	0.0135
850	0.7365	0.0533	0.0033	0.9449	0.2538	0.0075
900	0.6913	0.0588	−0.0009	0.9425	0.3068	0.0122
950	0.6273	0.0768	0.0025	0.9227	0.3682	0.0058

and covariance function parameters. The PErK software was used to perform these operations.[18]

With the parameters of the trend function and the covariance function estimated, the value of $\ln(t_f)$ was predicted at new locations u using the 183 evaluations of the two-grain crystal plasticity finite element model as training data. The response $Z(u) = \ln(t_f)$ was kriged on a $10 \times 10 \times 10 \times 10$ grid for the input variables SF, θ_{mis}, D and the applied load P. Figure 8 shows the kriged predictions of $Z(u) = \ln(t_f)$ on the colour scale (blue – short times-to-crack initiation, red – long times to crack initiation) and SF, θ_{mis} and D making up the coordinate axes. The plot is given for a specific value of $P = 750$ MPa as an example. In effect, the time-to-crack initiation is predicted as a function of the four-dimensional space of the input variables.

The accuracy of the kriging metamodel was assessed using cross validation. In cross validation, for a training data set with n samples, the value of $Z(s)$ was predicted at one of the training data sample locations using all of the *remaining* (n-1) locations to develop the kriging model. The process was repeated for each sample in the training data. Figure 9 presents a plot of the predicted value of $Z(s)$ with respect to the actual value. The coefficient of determination was calculated to be $R^2 = 0.99$.

Scatter plots - qualitative sensitivity analysis

The kriging surrogate was evaluated for 100 000 random samples of the input variables. Scatter plots of the time-to-crack-initiation are given with respect to each of the input variables in Figs 10–12 for an applied load of 750 MPa. The dominant variables controlling the variance of the response are visually identified as those exhibiting a noticeable trend with reduced scatter about the trend. Figure 10 shows a significant impact of SF on

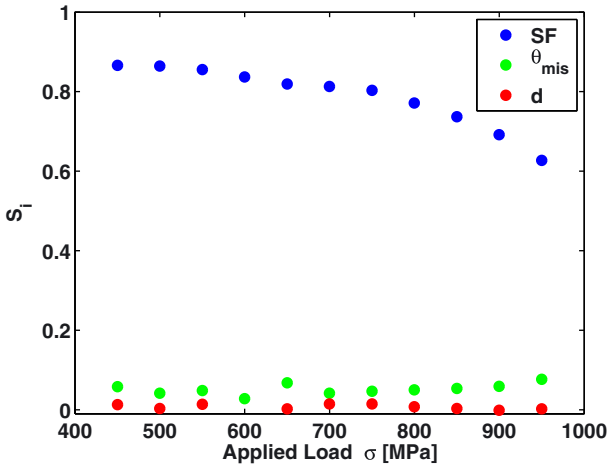

Fig. 14 First order sensitivity indices of $\ln(t_f)$ with respect to the applied load. The Schmid factor becomes less dominant as the load increases.

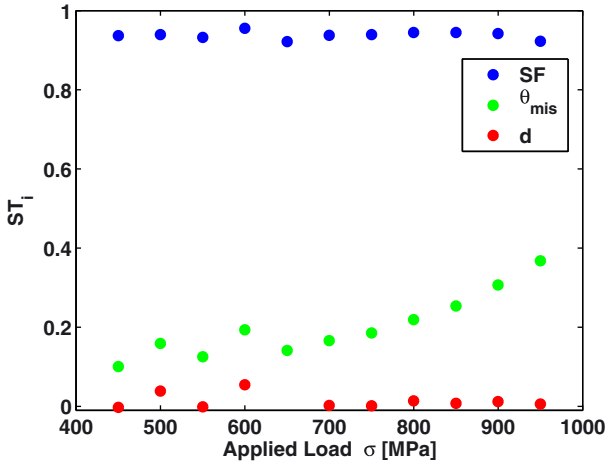

Fig. 15 Total effect sensitivity indices of $\ln(t_f)$ with respect to the applied load. The contribution of the misorientation angle to the variance of the crack initiation life increases as the load increases.

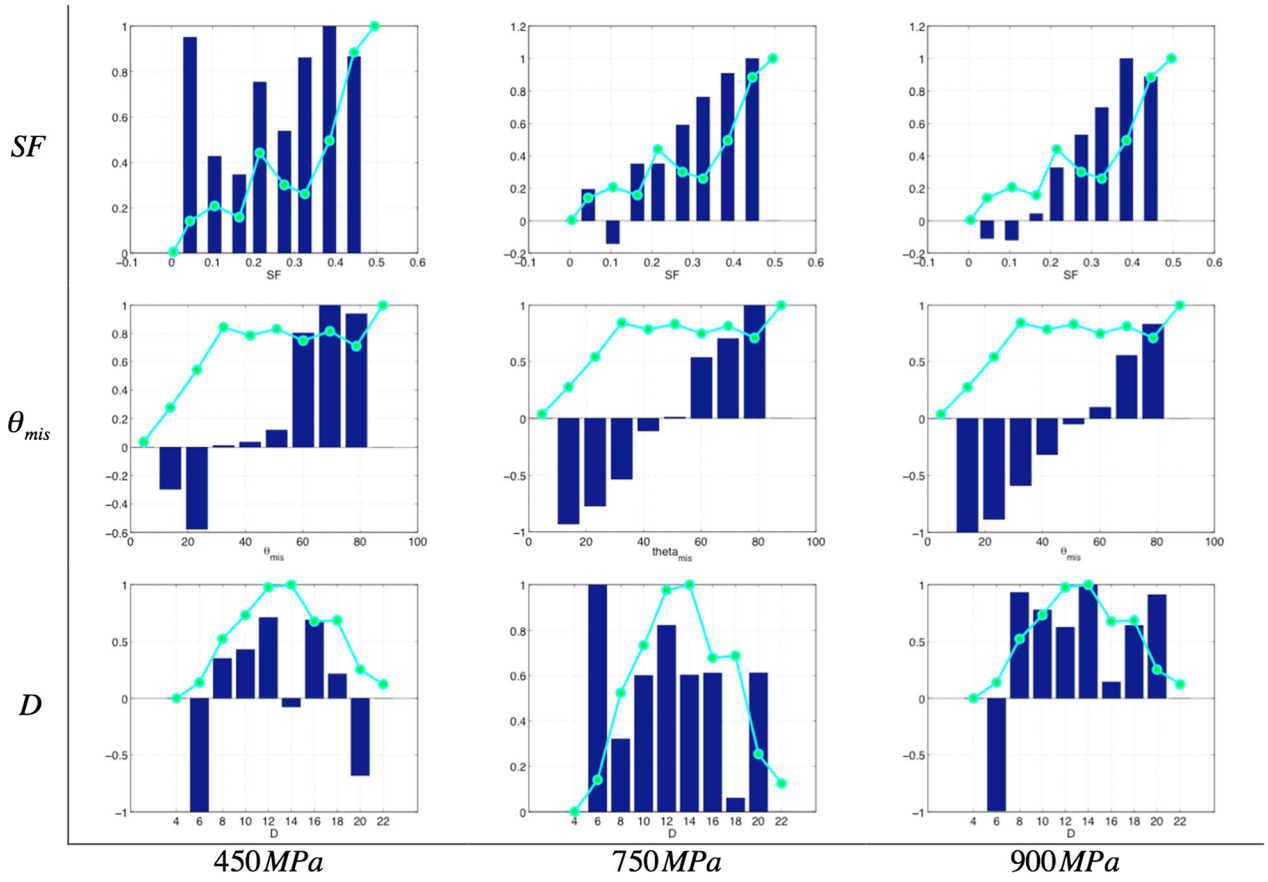

Fig. 16 Sensitivity of mean of $\ln(t_f)$ with respect to Schmid factor, misorientation angle and grain size for applied load 450, 750 and 900 MPa. Each blue bar is the value of the localised sensitivity of the mean with respect to the associated region of the input variable in the x-axis. Each green line with dot markers represents the normalised PDF of the input variable, allowing comparison with the sensitivities.

the trend and scatter of the time-to-crack-initiation. Figure 11 shows that θ_{mis} has a less pronounced impact on the trend and scatter of the response. Figure 12 shows that D has a minor role in the scatter of the response.

Certain regions of the input variables strongly determined the distribution of the response. In particular, higher values of the Schmid Factor resulted in reduced variance of the time-to-crack initiation.

Global sensitivity analysis

The sensitivity analysis was performed as described in the section on Kriging with $N = 100\,000$ for the random input variables SF, θ_{mis} and D. The applied load P was considered a deterministic variable in this analysis and set at various levels between 450–950 MPa. The mean and variance of the transformed time-to-crack-initiation tended to decrease as the load increased, as seen in Table 2 and Fig. 13.

Table 3 shows the global sensitivity analysis determined that the Schmid factor was the most important variable. For example, at $P = 450$ MPa, the numerical results indicate that the variance of the Schmid factor accounts for approximately 87% of the variance in the log-transformed time-to-crack initiation. The GSA-identified dominant variable matches that found from visually inspecting the scatter plots. The next most important variable was the misorientation angle, although its first-order index was about 5%, it has an appreciable total effect contribution, largely through its interaction with the Schmid factor. The global sensitivity analysis suggests that the variance of the grain size has little effect on the variance of the crack initiation life. Because the grain size effects are small, the total effects of the misorientation angle must be due to interaction with the Schmid factor of the soft grain. This was confirmed by calculating the second-order interaction effects indices. Figures 14 and 15 show the first-order index of SF decreasing and the total effects index of θ_{mis} increasing as the load increases.

Localised sensitivity analysis

The extent of the importance of 'regions' within the random variables was quantified with a localised sensitivity analysis. The normalised sensitivities of the mean and

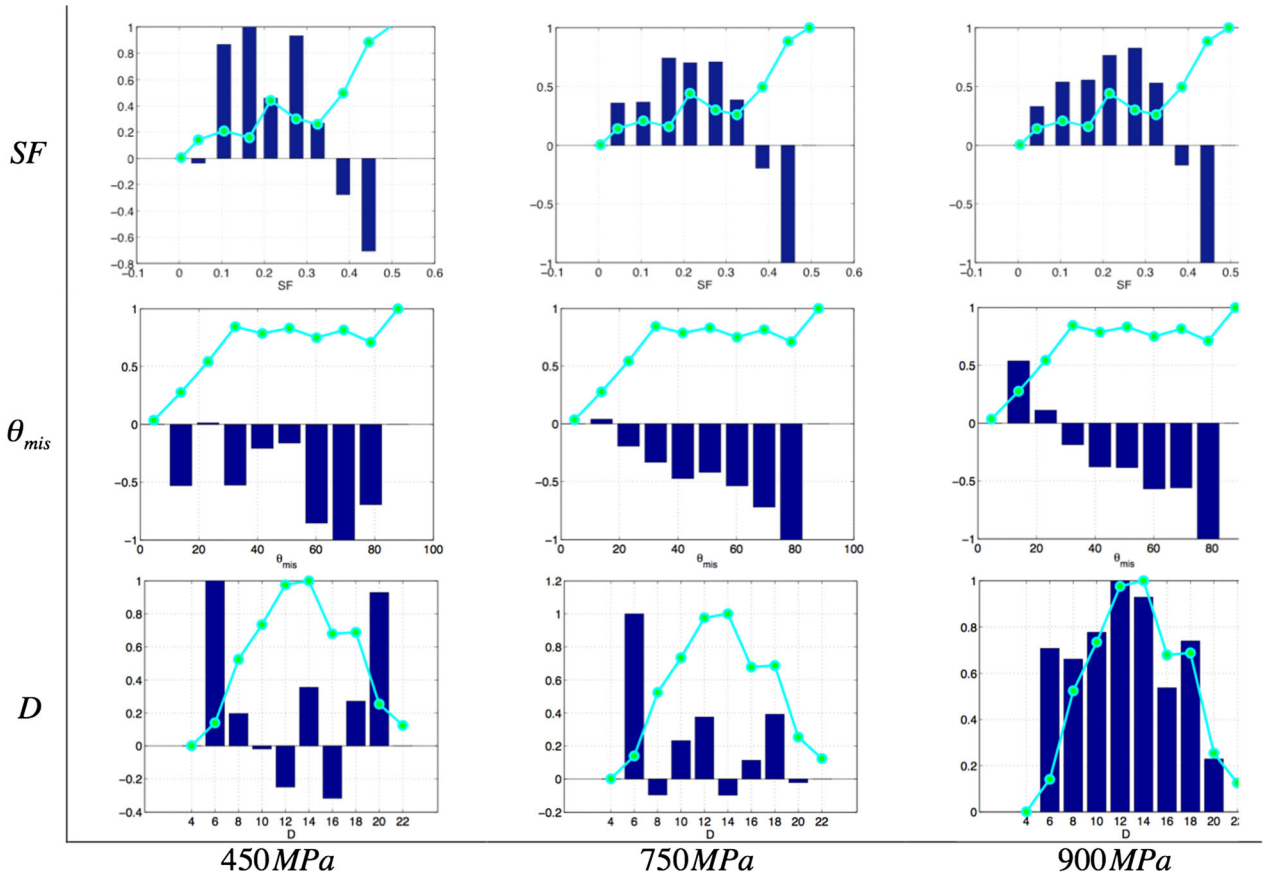

Fig. 17 Sensitivity of standard deviation of $\ln(t_f)$ with respect to Schmid factor, misorientation angle and grain size for applied load 450, 750 and 900 MPa. Each blue bar is the value of the localised sensitivity of the standard deviation with respect to the associated region of the input variable in the *x*-axis. Each green line with dot markers represents the normalised PDF of the input variable, allowing comparison with the sensitivities.

standard deviation of the log-transformed time-to-crack initiation are presented along with the PDF of each random variable in Figs 16 and 17 for applied loads of 450, 750 and 900 MPa.

Localised sensitivity analysis of the mean of $\ln(t_f)$

The localised sensitivity results for the Schmid factor are presented in Fig. 16 as a function of the applied loading. The results indicate that for loading values of 750 and 900 MPa, the mean of $\ln(t_f)$ is most sensitive to the region of high values of the Schmid factor. These results indicate that it is important to correctly characterise the right tail of the Schmid factor.

The localised sensitivity results for the misorientation angle are presented in Fig. 16. The mean of $\ln(t_f)$ is clearly most sensitive to the tails (right and left) of the misorientation angle; negative for the left tail, positive for the right tail.

The localised sensitivity results for the grain size are presented in Fig. 16. The effect of the regions of the distribution of the grain size on the mean of $\ln(t_f)$ is difficult to determine. This is due to the fact that, as shown by global sensitivity analysis, this random variable has such a small effect (relative to the crystallographic orientation factors), thus the number of Monte Carlo samples used to compute the local sensitivity would have to be increased significantly to accurately assess the local sensitivities.

Localised sensitivity analysis of the standard deviation of $\ln(t_f)$

The localised sensitivity results with respect to the standard deviation of $\ln(t_f)$ are presented in Fig. 17. The results indicate that the central region and far right tail are most significant for the Schmid factor. For the misorientation angle, the right tail is most significant. Results for the grain size are inconclusive until the load equals 900 MPa. At this load level, it is clear that most regions of the distribution are equally important.

Summary discussion

These results show that the maximal basal Schmid factor of the soft grain was the most important variable

of the variables considered affecting the load shedding-induced crack initiation life of Ti-6242. It was also found that the neighbouring grain size was less important than the crystallographic orientation factors to crack formation life. This section discusses these findings and compares them with experimental observations in the literature.

The large magnitudes of the localised sensitivity for the mean and standard deviation of the crack initiation life with respect to the right tail of the Schmid factor suggest a softer neighbouring grain (large *SF*) will result on average in shorter crack initiation life and larger variance in the life. These results support observations in the literature that a dominant mode of crack initiation in the alpha grains of titanium alloys involves a hard oriented region neighboured by a soft oriented region.[7,10,20,24,25] In particular, this study suggests that the *variance* of the Schmid factor of the neighbouring soft grain plays a significant role in the *variance* of the crack initiation life.

There are many examples in the literature that the grain size of the bulk material affects the deformation, strength and life response of polycrystalline materials. For instance, in equiaxed Ti-6Al-4V, larger mean grain size typically results in shorter fatigue life.[2] There is evidence that the size of grains local to facet sites is important to crack formation. For example, recent investigation[23] of slip-induced microcracks in Ti-6246 has shown that the sizes of faceted grains are slightly larger than the rest of the material. Previous numerical studies of load shedding in a hard–soft grain combination have reached contradicting conclusions that either the effect of hard grain size is not significant[15] or is significant[7]. In Ref. [15], it was claimed that the size of the soft grain has a significant impact on the stresses in the hard grain. In Ref. [7], as the size of the hard grain changed, the size of the soft grain matrix changed simultaneously (because of a constant ensemble volume); the noted impact on stresses in the hard grain is possibly due to the change in soft grain size.

In this study of load shedding-induced microcracks, the size of the hard-oriented grain was not considered a random variable, and its importance was not assessed. Instead, we used probabilistic methods to explicitly examine the size of the soft-oriented grain *neighbouring* the potential crack formation site of the hard-oriented grain. It was found that the distribution of the neighbouring soft grain size has a smaller effect on the distribution of crack formation life than crystallographic orientation factors. We emphasise that for a given hard-oriented grain, the effect of the soft-oriented grain size on crack formation life is not zero, just smaller than that of the soft grain maximal basal Schmid factor and misorientation angle.

CONCLUSION

A probabilistic sensitivity analysis of the time to crack initiation of a pair of alpha grains of Ti-6242 was implemented with the Schmid factor, the misorientation angle and the grain size as random variables. A Monte Carlo sampling method was enabled by the development of a kriging metamodel. The kriging metamodel allowed for many samples to be evaluated efficiently for the time-to-crack-initiation. The probabilistic sensitivity analysis revealed several important findings for load-shedding induced crack formation life.

- The Schmid factor of the soft grain was by far the dominant variable, that is, variation in Schmid factor largely determined the variation in the time-to-crack initiation.
- The misorientation angle on its own is less important than its interaction with the soft grain Schmid factor.
- Increasing load tends to reduce the dominance of the Schmid factor, but this variable is still dominant.
- Increasing load tends to increase the importance of θ_{mis}'s interaction with the Schmid factor.
- The soft grain size has a comparatively lower influence.

The localised sensitivity analysis suggests that the mean of the crack initiation life

- is more sensitive to the right tail of the Schmid factor; and
- is more sensitive to the tails of the misorientation angle than the centre.

The localised sensitivity analysis suggests that the standard deviation of the crack initiation life

- is more sensitive to the right tail and centre region of *SF*; and
- is more sensitive to the right tail misorientation angles.

The probabilistic sensitivity analysis investigated how changes to the *distribution* of the microstructural variables affects the *distribution* of the creep and dwell fatigue crack initiation life. By accounting for the inherent variability of the microstructural variables, the results give a stronger argument for the contribution of the neighbouring soft-basal-slip-oriented grain to crack nucleation life in some titanium alloys.

The results from this two-grain numerical study agree with experimental results for the bulk material. This suggests it may be possible to make other conclusions about the bulk material with two-grain microstructural model results. The probabilistic sensitivity methodology used for this two-grain model could be generalised to include more of the local neighbourhood of grains to examine the contribution of their interaction on the crack formation life.

Acknowledgements

The authors acknowledge the financial support provided by AFOSR Grant FA9550-09-1-0452, David Stargel, Program Manager, and the National Science Foundation (HRD-0932339) through the CREST Center for Simulation, Visualization and Real Time Computing. The authors thank Miguel Cortina for the use of the localised sensitivity code for the relevant analysis in the section on Results and Discussion section.

REFERENCES

1 Sinha, V., Mills, M. J. and Williams, J. C. 2004 Understanding the contributions of normal-fatigue and static loading to the dwell fatigue in a near-alpha titanium alloy. *Metall. Mater. Trans. A*, **35A**, 3141–3148.
2 Lutjering, G. and Williams, J. C., Titanium, 2nd ed., Springer: New York, 2007.
3 Hasija, V., Ghosh, S., Mills, M. and Joseph, D. (2003) Deformation and creep modeling in polycrystalline Ti-6Al alloys. *Acta Mater.*, **51**, 4533–4549.
4 Bache, M. R., Evans, W. J., Randle, V. and Wilson, R. J. (1998) Characterization of mechanical anisotropy in titanium alloys. *Mater. Sci. Eng.*, **A257**, 139–144.
5 Littlewood, P. D. and Wilkinson, A. J. (2012) Local deformation patterns in Ti-6Al-4V under tensile, fatigue, and dwell fatigue loading. *Int. J. Fatigue*, **43**, 111–119.
6 Chan, K. S. (2010) Roles of microstructure in fatigue crack initiation. *Int. J. Fatigue*, **32**, 1428–1447.
7 Dunne, F. P. E., Walker, A. and Rugg, D. (2007) A systematic study of hcp crystal orientation and morphology effects in polycrystal deformation and fatigue. *Proc. R. Soc. A*, **463**, 1467–1489.
8 Dunne, F. P. E. and Rugg, D. (2008) On the mechanisms of fatigue facet nucleation in titanium alloys. *Fatigue Fract. Eng. Mater. Struct.*, **31**, 949–958.
9 Anahid, M., Samal, M. K. and Ghosh, S. (2011) Dwell fatigue crack nucleation model based on crystal plasticity finite element simulations of polycrystalline titanium alloys. *J. Mech. Phys. Solids*, **59**, 2157–2176.
10 Sinha, V., Spowart, J. E., Mills, M. J. and Williams, J. C. (2011) Observations on the faceted initiation site in the dwell-fatigue tested Ti-6242 alloy: crystallographic orientation and size effects. *Metall. Mater. Trans. A*, **37A**, 1507–1518.
11 Millwater, H. R. (2009) Universal properties of kernel functions for probabilistic sensitivity analysis. *Probab. Eng. Mech.*, **24**, 89–99.
12 Saltelli, A., Ratto, M., Andres, T., Campolongo, F., Cariboni, J., Gatelli, D., Saisana, M., Tarantola, S. Global Sensitivity Analysis: The Primer. England, John Wiley & Sons Ltd, 2008, 160–165.
13 Millwater, H., Singh, G. and Cortina, M. (2011) Development of a localized probabilistic sensitivity method to determine random variable regional importance. *Reliab. Eng. Syst. Saf.*, **107**, 3–15.
14 Deka, D., Joseph, D. S., Ghosh, S. and Mills, M. J. (2006) Crystal plasticity modeling of deformation and creep in polycrystalline Ti-6242. *Metall. Mater. Trans. A*, **17A**, 1371–1388.
15 Venkatramani, G., Ghosh, S. and Mills, M. J. (2007) A size dependent crystal plasticity finite element model for creep and load-shedding in polycrystalline titanium alloys. *Acta Mater.*, **55**, 3971–3986.
16 Ghosh, S., Anahid, M. and Chakraborty, P. (2011) Modeling fatigue crack nucleation using crystal plasticity finite element simulations and multi-time scaling. In: Computational Methods for Microstructure-Property Relations, S. Ghosh & D. Dimiduk (co-editors), NY, Springer, 497–554.
17 Cressie, N., Statistics for Spatial Data. New York, John Wiley & Sons Ltd, 1993.
18 Santner, T. J., Williams, B. J. and Notz, W., The Design and Analysis of Computer Experiments. Springer Series in Statistics. Springer-Verlag, Inc., New York, 2003.
19 Martin, J. D. and Simpson, T. W. (2005) Use of kriging models to approximate deterministic computer models. *AIAA J.*, **43**, 853–863.
20 Bieler, T., Goetz, R. L. and Semiatin, S. L. (2005) Anisotropic plasticity and cavity growth during upset forging of Ti-6Al-4V. *Mater. Sci. Eng. A*, **405**, 201–213.
21 Kirane, K. and Ghosh, S. (2008) A cold dwell fatigue crack nucleation criterion for polycrystalline Ti-6242 using grain-level crystal plasticity FE model. *Int. J. Fatigue*, **30**, 2127–2139.
22 Sackett, E. E., Germain L. and Bache M. R. (2007) Crystal plasticity, fatigue crack initiation and fatigue performance of advanced titanium alloys. *Int. J. Fatigue*, **29**, 2015–2021.
23 Szczepanski, C. J., Jha, S. K., Larsen, J. M. and Jones, J. W. (2008) Microstructural influences on very-high-cycle fatigue-crack initiation in Ti-6246. *Metall. Mater. Trans. A*, **39A**, 2841–2851.
24 Bache, M. R. (2003) A review of dwell sensitive fatigue in titanium alloys: the role of microstructure, texture and operating conditions. *Int. J. Fatigue*, **25**, 1079–1087.
25 Evans, W. J. and Bache, M. R. (1994) Dwell-sensitive fatigue under biaxial loads in the near-alpha titanium alloy IMI685. *Fatigue*, **16**, 443–452.